Time-reversal symmetry breaking in the Fe-chalcogenide superconductors

Nader Zaki[a], Genda Gu[a], Alexei Tsvelik[a], Congjun Wu[b], and Peter D. Johnson[a,1]

[a]Condensed Matter Physics and Materials Science Division (CMPMSD), Brookhaven National Laboratory, Upton, NY 11973; and [b]Department of Physics, University of California, San Diego, CA 92093

Edited by J. C. Séamus Davis, University College Cork, Cork, Ireland, and approved November 25, 2020 (received for review April 20, 2020)

Topological superconductivity has been sought in a variety of heterostructure systems, the interest being that a material displaying such a phenomenon could prove to be the ideal platform to support Majorana fermions, which in turn could be the basis for advanced qubit technologies. Recently, the high-T_c family of superconductors, $FeTe_{1-x}Se_x$, have been shown to exhibit the property of topological superconductivity and further, evidence has been found for the presence of Majorana fermions. We have studied the interplay of topology, magnetism, and superconductivity in the $FeTe_{1-x}Se_x$ family using high-resolution laser-based photoemission. At the bulk superconducting transition, a gap opens at the chemical potential as expected. However, a second gap is observed to open at the Dirac point in the topological surface state. The associated mass acquisition in the topological state points to time-reversal symmetry breaking, probably associated with the formation of ferromagnetism in the surface layer. The presence of intrinsic ferromagnetism combined with strong spin–orbit coupling provides an ideal platform for a range of exotic topological phenomena.

superconductivity | topology | magnetism

Magnetism and superconductivity represent emergent ground states in condensed-matter systems that often compete. In the high-T_c cuprates for example, the phase diagram is characterized by magnetism at low doping and superconductivity at higher doping levels (1). There is some tendency for these two regions to overlap in the related Fe-based superconductors but note that the magnetic ground state is antiferromagnetic with neighboring spins antiparallel as in the configuration associated with the Cooper pairs in spin-singlet superconductivity (2). Ferromagnetism on the other hand with neighboring spins aligned parallel most definitely appears to counter the possibility of the normal spin alignment associated with superconductivity, at least for systems characterized by singlet pairing. However, the spin–orbit interaction associated with the formation of protected surface electron states on the surface of topological insulators can also play a role, a recent example being the demonstration that the high-T_c superconductors, $FeTe_{1-x}Se_x$, supports topological surface states (3, 4) reflecting the large spin–orbit interaction on the ligand Te atoms (5). Indeed, in our own studies of this system we showed that spin–orbit effects (5) combined with the local moments (4) associated with the paramagnetic state resulted in an inverted gap at the zone boundary capable of supporting a topological state. In the present study, we examine the interaction between magnetism, superconductivity, and topology in this fascinating and complex system. With the superconducting transition we observe a gap opening at the chemical potential, a characteristic of superconductivity reflecting the formation of Cooper pairs but, with the same transition, we also find evidence of a second gap opening, now at the Dirac point associated with the topological surface state. The discovery of mass acquisition associated with the superconducting transition points to the breaking of a symmetry associated with the topological state. In fact, with only a single cone at the center of the Brillouin zone the observation of mass acquisition leads to the conclusion that time-reversal symmetry is broken, consistent with the development of some form of magnetic order. Ferromagnetism will break time-reversal symmetry; antiferromagnetism will not. The observation of spontaneous time-reversal symmetry breaking may well bring helpful information to our understanding of the symmetry of the superconducting gap function in such systems (6). The development of ferromagnetism is also highly suggestive that in the superconducting state this system could prove an ideal platform for the demonstration of a range of exotic topological phenomena. Indeed it has recently been suggested that in the presence of an external magnetic-field topological superconductivity with a Dirac gap and the half quantum anomalous Hall state can be competing ground states (7). Further the same theory suggests that Majorana modes will exist on the boundary of such regions. It is possible that topological superconductors supporting such chiral edge modes could also exhibit a quantized thermal Hall conductance.

Results

In Fig. 1*A* we show the photoemitted spectral intensity from $FeTe_{0.7}Se_{0.3}$ in the normal state. The intensity is obtained by summing the individual spectral intensities obtained with orthogonal light polarizations that effectively removes any matrix element effects. As in previous studies, the plot is characterized by two features, the bulk band dispersing downward away from the Γ-point and the topological state represented by the conelike structure dispersing upward from the Dirac point. Previous

Significance

In the Fe-chalcogenide superconductors, topology, superconductivity, and magnetism all come together to provide a platform for a range of exotic quantum phenomena. Topology and superconductivity can interact to give topological superconductivity capable of supporting Majorana fermions that could prove to be the basis of future qubit technology. The large spin–orbit interaction associated with the topological phenomena combined with magnetism can potentially result in the quantum anomalous Hall effect although the superconductivity will work against such. It is important that we understand the relevant roles of the different phenomena. Here we provide evidence of time-reversal symmetry breaking and associated mass acquisition in a topological surface state at the superconducting transition, an observation highly suggestive of the formation of surface ferromagnetism.

Author contributions: P.D.J. designed research; N.Z., G.G., A.T., and C.W. performed research; N.Z. and P.D.J. analyzed data; and C.W. and P.D.J. wrote the paper with important contributions from all authors including theoretical input from A.T. and C.W.

The authors declare no competing interest.

This article is a PNAS Direct Submission.

[1]To whom correspondence may be addressed. Email: pdj@bnl.gov.

This article contains supporting information online at https://www.pnas.org/lookup/suppl/doi:10.1073/pnas.2007241118/-/DCSupplemental.

Published January 12, 2021.

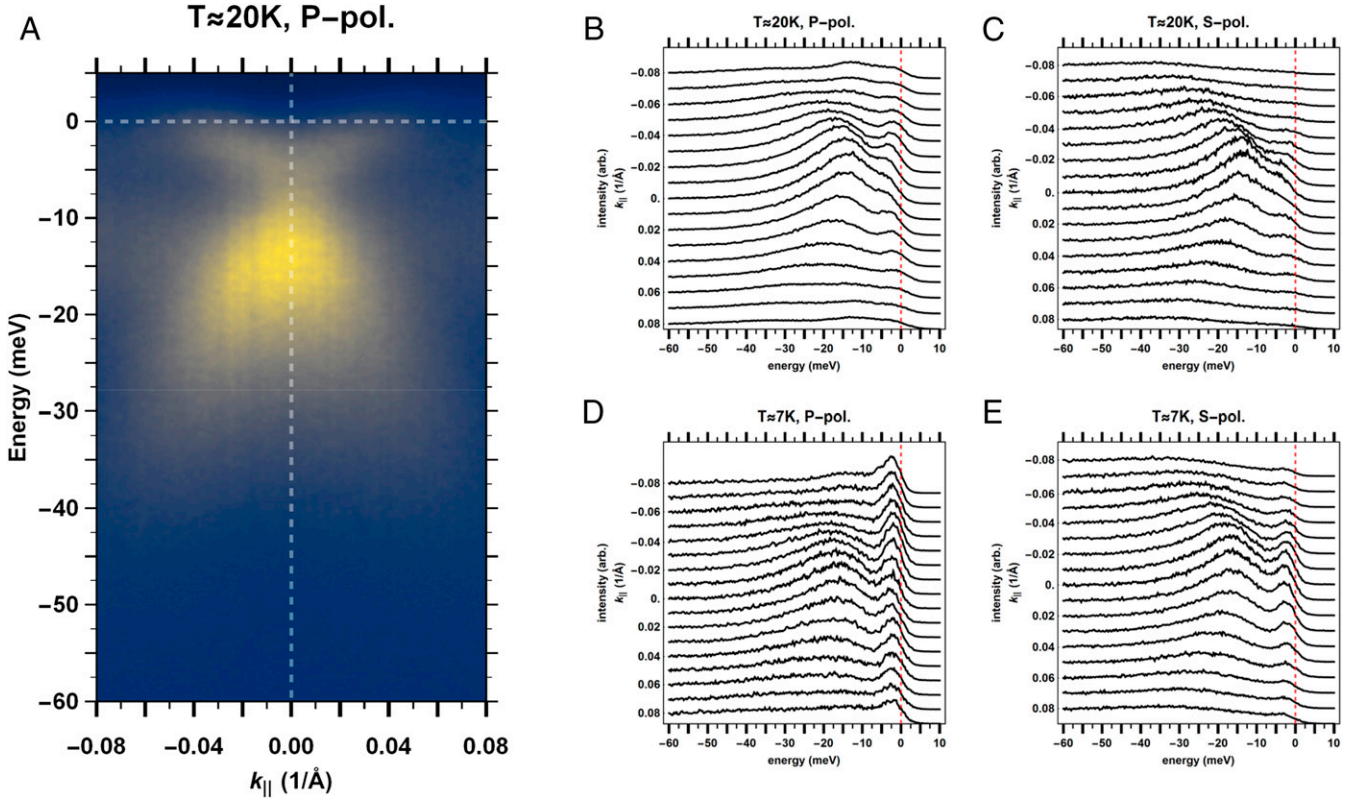

Fig. 1. Photoemitted spectral intensities measured in the normal and superconducting states. (*A*) Spectral intensity measured in the vicinity of the Γ-point ($k_{||} = 0$) from $FeTe_{0.7}Se_{0.3}$. The total intensity corresponds to the sum of those intensities measured with incident p-polarized and s-polarized light. (*B*) Energy distribution curves measured in a region ± 0.08 Å around the Γ-point from $FeTe_{0.7}Se_{0.3}$ using p-polarized light and with the sample in the normal state at 20 K. (*C*) The same as in *B* but now with s-polarized light. *D* and *E* are, respectively, the same as *B* and *C* but now with the sample held in the superconducting state at 6 K.

studies of the Dirac cone have demonstrated the helical spin structure associated with the state using either spin-polarized photoemission with linearly polarized incident light (4) or photoemission with circularly polarized incident light (5). In Fig. 1 we also show the photoemission spectra recorded from the material near the center of the zone as a function of the incident light polarization and temperature, corresponding in Fig. 1, *B* and *C,* to the normal state and in Fig. 1, *D* and *E*, to the superconducting state. In the latter spectra, the development of the peak associated with the superconducting transition is clearly visible for p-polarized light across the entire range of $k_{||}$ measured. For s-polarized light, on the other hand, the onset of superconductivity is only visible in the vicinity of the topological state at the center of the zone. It is important to note that these studies benefit from the high spatial resolution, <20 μm, in that the samples display inhomogeneities on length scales of 50 μm or less. In the appropriate geometry, matrix element effects in the photoemission process allow, in principle, the identification of the orbital character of the initial state (*SI Appendix*, section 2). In the present case, the observation that the state associated with the superconducting transition is evident only with p-polarized light could suggest that the onset of superconductivity is orbital selective. Indeed in studies of a related system, $FeSe_{0.4}Te_{0.6}$, a spectroscopic imaging scanning tunneling microscopy (SI-STM) study reported evidence for orbital ordering which the authors correlated with superconductivity (8). Orbital ordering (9) or selectivity (10) has also been invoked in a separate SI-STM and associated theoretical studies of the related FeSe. Here we comment that in our earlier study we proposed that spin–orbit coupling hybridizes the d_{xz} and d_{yz} orbitals in these materials. Thus the spin–orbit coupling results in two bands, α_1 and α_2, split by the energy of the coupling strength aligning orbital angular momentum and spin around the Γ-point (4). Thus the α_1 band will have Kramers degenerate contributions given by $(d_{xz} + id_{yz})|\uparrow>$ and $(d_{xz} - id_{yz})|\downarrow>$ and the α_2 band by $(d_{xz} + id_{yz})|\downarrow>$ and $(d_{xz} - id_{yz})|\uparrow>$.

We make one further observation relating to the peak associated with the superconducting state as observed in the spectrum taken with p-polarized light. As noted, it is observed across the entire zone center. This represents unusual behavior as pointed out in an earlier study of superconductivity in the material $Fe_{1+y}Se_xTe_{1-x}$, where the possibility of a Bose–Einstein condensation (BEC)-type transition as opposed to a Bardeen Cooper Schrieffer (BCS)-type transition was discussed (11). The authors of that study noted that a BEC transition would result in a superfluid peak at $q = 0$ or the center of the zone as observed in the present study. A peak at the center of the zone contrasts with the BCS mechanism where we expect to see the Bogolyubov quasiparticles showing their peak intensity around k_F away from the zone center. As noted by the authors of ref. 11, the cross-over from BCS to BEC behavior reflects the ratio of Δ/E_F where again Δ represents the superconducting gap and E_F is the Fermi energy. The Bogolyubov dispersion associated with pairing in the topological state would be expected to disperse downward at the Fermi wave-vector crossing of ∼0.03 $Å^{-1}$ and away from the zone center. The dispersion associated with pairing in the bulk α_2-band could potentially initially disperse toward the zone center but the Fermi crossing for that band is much further out at ∼0.15 $Å^{-1}$ (5). We further note that evidence for BCS–BEC cross-over behavior has also been reported in a recent study of the related

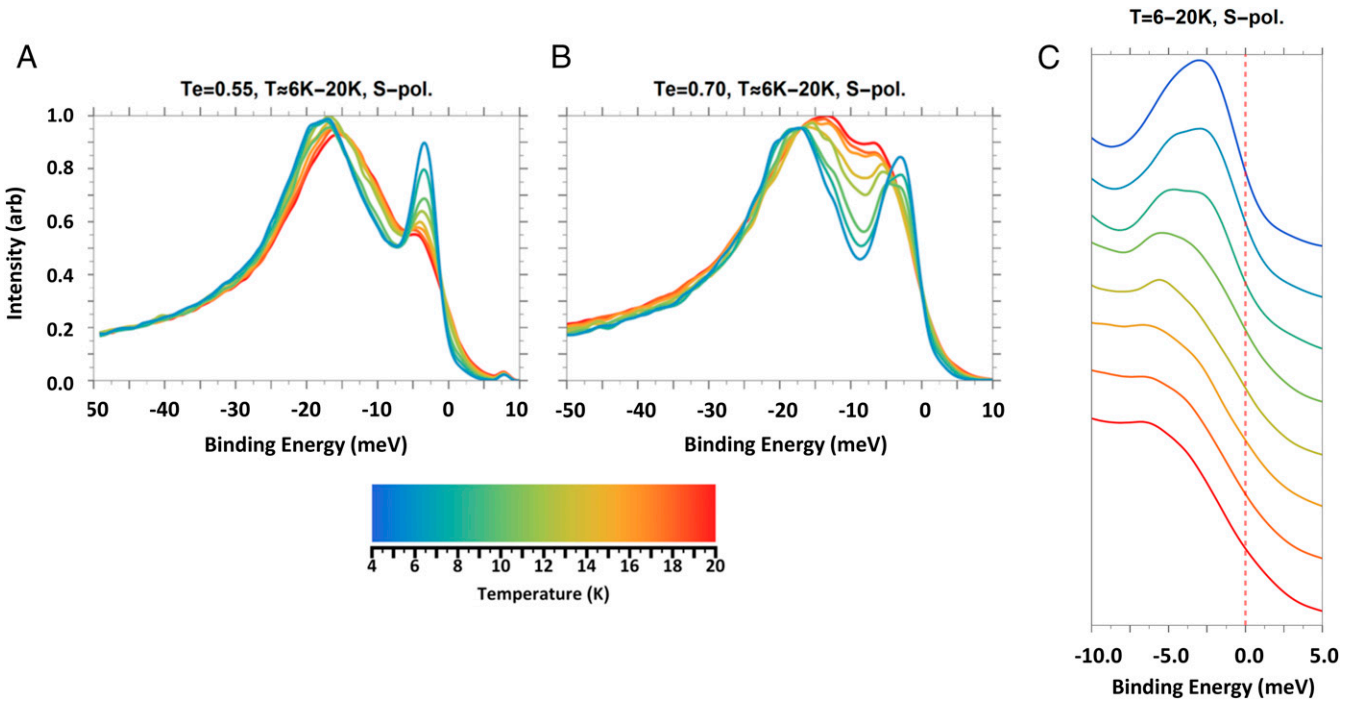

Fig. 2. Temperature dependence of the photoemission spectra along the surface normal. *A* and *B* represent the temperature dependence from 20 to 6 K of the measured spectra recorded along the surface normal from $FeTe_{0.55}Se_{0.45}$ and $FeTe_{0.7}Se_{0.3}$, respectively. *C* shows an expanded view of the temperature dependence of the peak immediately below the Fermi level for the spectra in *B*.

FeSe system (12). Here we simply note that the properties of the topological surface state at the center of the zone are highlighted by the use of incident s-polarized light and the properties of the bulk superconductivity away from the zone center by the use of incident p-polarized light We therefore chose to use s-polarized incident light to examine the properties of the topological state in detail.

Fig. 2 compares the temperature dependence of the photoemission spectra recorded along the surface normal, corresponding to $k_{||} = 0$, using s-polarized light for temperatures from 20 K down through the superconducting transition at $T_c = 14.5$ to 6 K, well into the superconducting state for (*A*) $FeTe_{0.55}Se_{0.45}$ and (*B*) $FeTe_{0.7}Se_{0.3}$. However, there are notable differences between the two systems presented in Fig. 2. At 20 K the increase in Te concentration on moving from $Te_{0.55}$ to $Te_{0.7}$ results in an increase in the intensity of the peak in the vicinity of the Dirac point, clearly showing the latter is related to the Te concentration. With the development of superconductivity, although more obvious in the 70% Te material, in both cases the two most prominent features in the spectra appear to be pushed apart as the temperature goes below the bulk T_c; the one at lower binding energy moving toward the chemical potential and the second at a binding energy beyond the Dirac point (located ~8.0 meV below the chemical potential as discussed in *SI Appendix*) being pushed to higher binding energy. However, there are also differences between the peaks at low binding energy in the two systems. The peak in *A* is sharper with a width probably determined by the overall experimental resolution of 2.5 meV. The peak in *B* on the other hand is broader with a substructure suggesting the presence of more than one peak. Fig. 2*C* focuses specifically on the peak closer to E_F in Fig. 2*C* over the same temperature range. The peak again continuously changes its structure, indicating different components, one appearing to have its development associated with the superconducting transition. This is particularly noticeable in the 10 K spectrum where at least two peaks are clearly resolved.

The spectra in Fig. 2*A* could be interpreted simply as the development of a peak associated with the superconducting transition as is evidenced in many superconducting materials. Indeed, in Fig. 3 we plot the temperature dependence of the

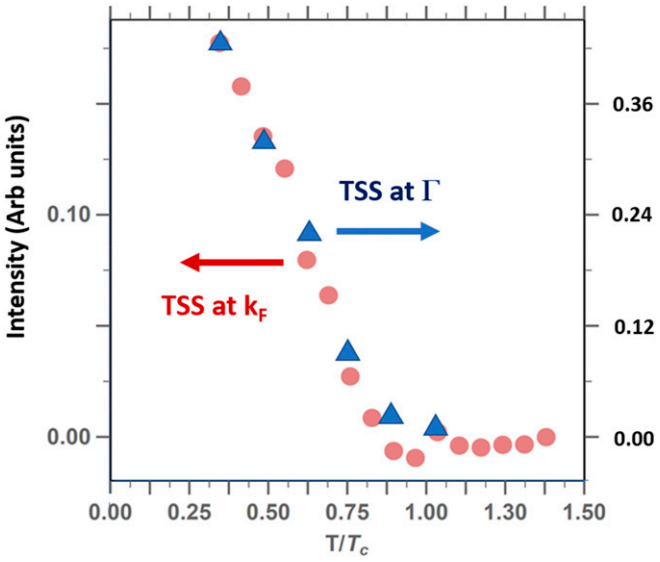

Fig. 3. Measured intensity in the TSS observed on $FeTe_{0.55}Se_{0.45}$ as a function of momentum. The intensity of the TSS is compared at two points, Γ (maroon circles) and k_F (blue triangles). In both cases the intensity is normalized to the intensity of the d band at the center of the Brillouin zone. Note the difference in the intensity scales, k_F on the left-hand side and Γ on the right-hand side.

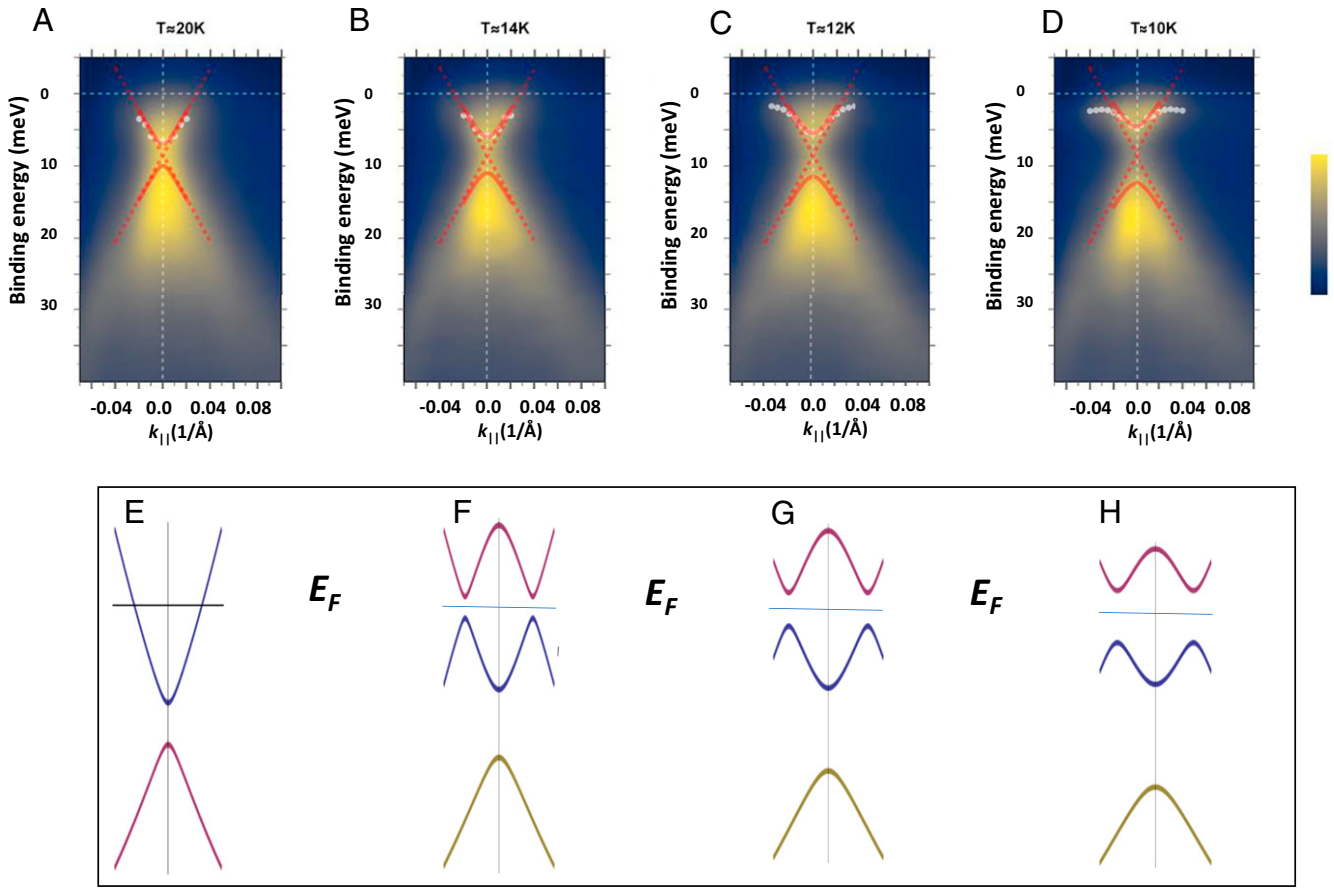

Fig. 4. Measured dispersions in the vicinity of the Γ-point as a function of temperature. Spectral intensity measured in the vicinity of the Γ-point as a function of temperature. *A–D* correspond to 20, 14, 12, and 10 K, respectively. Superimposed over the measured intensities, the white dotted curves show the peak intensities, the red dashed curve shows the underlying Dirac cone, and the solid red curves show the Dirac cone but now with a gap at the Dirac point determined by fitting with Eq. **4**. (*E–H*) The calculated equivalent of *A–D* using the expression given in Eq. **3**.

peak observed at the Γ-point for $FeTe_{0.55}Se_{0.45}$ as a function of temperature and compare that with the intensity of the superconducting peak at k_F. They are clearly both linked to the superconducting transition. However, the density of photoemission initial states at a given energy E in the vicinity of a gap has an energy dependence given by $E/(E^2-m^2)^{1/2}$ where $2m$ is the magnitude of the gap (*SI Appendix*, section 4). Thus the photoemission intensity peaks at the gap edge and decreases as one moves away from the gap. This is particularly evident in Fig. 1*E* where the topological surface state (TSS) is most intense at the center of the zone and then falls off in intensity as the state disperses upward toward the Fermi crossing at k_F. Fig. 3 further confirms this picture. As we discuss below, these observations point to the formation of two gaps associated with the superconducting transition, one at the chemical potential, and a second gap at higher energies, namely at the Dirac point.

Analysis and Conclusions. In Fig. 4 we show a series of measured spectral intensities at the center of the zone, as a function of temperature above and below the superconducting transition. The spectral images clearly show the opening of a gap at the Dirac point at the transition temperature T_c. as is more evident in a movie we present in *SI Appendix*, Movie S1). In the latter showing the spectral response as a function of temperature from 20 K down through T_c to 5 K, the opening of two gaps, one at the chemical potential and one at the Dirac point, at the superconducting transition is very obvious. However, as we have discussed elsewhere, there is already a small gap at the Dirac point above T_c in the normal state (4). This gap may reflect superconducting fluctuations above T_c (6) (*SI Appendix*, section 6). Indeed, NMR and transport measurements provide some evidence of a pseudogap associated with preformed pairs with an onset T* of 20 K well above the Tc of 8 K in the related material FeSe (12). An alternative explanation would be the magnetic ordering of local moments in the surface layer as observed in a previous study of a doped topological insulator, also in the paramagnetic state in the bulk (13).

As noted earlier, the development of a larger temperature-dependent gap at the Dirac point and associated mass acquisition is an indicator of some form of time-reversal symmetry breaking associated with the bulk superconducting transition. To investigate this further we start with the assumption that the observed electron spectrum at the surface has only one Fermi pocket. This is different from the bulk, where the Fermi surface has multiple sheets. Hence the surface quasiparticles can be described by $\psi_\sigma(\mathbf{k})$, $\psi^+_\sigma(\mathbf{k})$, where σ represents the index of a "Kramers doublet," or, an "effective spin" and **k,** the two-dimensional momentum. Since photoemission shows well-defined quasiparticle excitations, we treat them as surface modes not propagating into the bulk. Furthermore, the mass term for a single Dirac cone (Weyl fermion) breaks time reversal and therefore requires an internal magnetic field. Another important factor is the strong spin–orbit coupling, λ, caused presumably by the strong electric field on the surface (the Rashba effect).

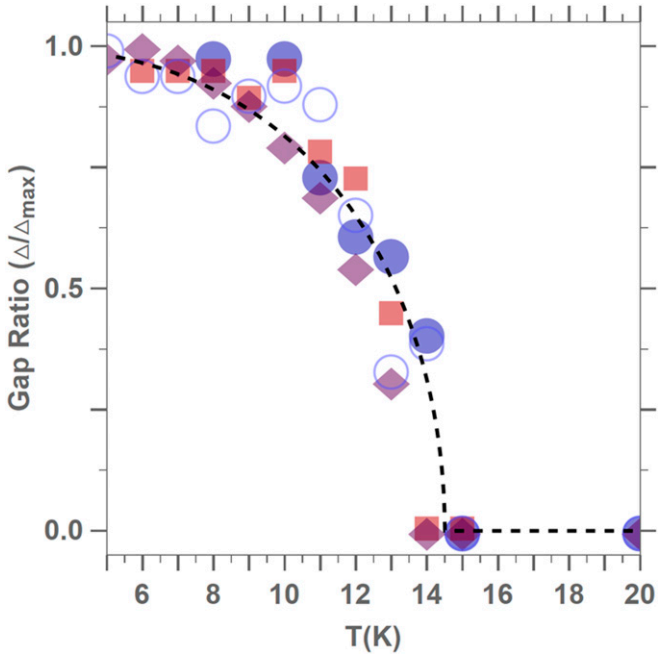

Fig. 5. Temperature dependence of the different gap magnitudes. Temperature dependence of the superconducting gap (red squares) from Ref. 3 and from the present study (purple diamonds) for the $Te_{0.55}$ system and the gap at the Dirac point from the present study for $Te_{0.55}$ (open circles) and $Te_{0.7}$ (blue circles) compared with the temperature dependence of the bulk superconductivity for the α_2 band (dashed line) as determined in Ref. 17.

We therefore use a model that represents the continuum limit of the model adopted by Mascot et al. (14).

The standard approach to the description of superconductivity is to use the Nambu notation (*SI Appendix*, section 5). Thus we introduce the Nambu spinor $\Psi^T(k) = (c_\uparrow(k), c_\downarrow(k), c_\downarrow^+(-k), c_\uparrow^+(-k))$, so that the Hamiltonian H is given by

$$H = \sum_k \hat{\Psi}^+(k)\hat{H}(k)\hat{\Psi}(k), \qquad [1]$$

where the Hamiltonian can be written as

$$\begin{aligned} H(k) = \quad & \varepsilon(k)\tau^z \otimes I + \lambda\tau^z \otimes \left(k_y\sigma^x - k_x\sigma^y\right) + h\tau^z \otimes \sigma^z \\ & + (Re\Delta)\tau^x \otimes I + (Im\Delta)\tau^y \otimes I. \end{aligned} \qquad [2]$$

Here the Pauli matrices τ^z act in the particle–hole space and the σ^z matrices act in the spin space. $\varepsilon_0(k) = k^2/2m$, the bare dispersion, μ is the binding energy of the Dirac point, and h the Weiss field generated by the presumed ferromagnetic ordering in the surface region. Diagonalizing Eq. **2** results in the energy spectrum (*SI Appendix*, section 5):

$$\begin{aligned} E_\pm^2 = & (\varepsilon_0(k) - \mu)^2 + \lambda^2k^2 + h^2 + \Delta^2k^2 \\ & \pm 2\left[(\varepsilon_0(k) - \mu)^2\left(\lambda^2k^2 + h^2\right) + \left|\Delta\right|^2\lambda^2k^4\right]^{1/2}. \end{aligned} \qquad [3]$$

In the vicinity of the Dirac point, well removed from the chemical potential, Eq. **3** reduces to $E_\pm = (\varepsilon_0(k) - \mu) \pm \sqrt{\lambda^2k^2 + h^2}$. Thus to get some idea of the magnitude of the magnetic field h we fit the measured dispersion in the vicinity of the Dirac point with the expression

$$E_\pm = \pm\sqrt{\lambda^2k^2 + h^2}. \qquad [4]$$

We could have simply made the assumption that the gap has the magnitude $2h$. However, we believe that the close proximity of the bulk bands to the bottom of the gap renders such an approach less accurate.

Fitting the measured spectral plots as shown in Fig. 4*A* provides us with a measure of h(T), the temperature dependence of the gap at the Dirac point. At the lowest temperatures the full opening of the gap is of the order of 8 meV. However, as noted earlier a gap of ~3.0 meV exists above Tc. We therefore associate the additional 5.0 meV with the development of superconductivity. By contrast, the full gap at the chemical potential directly associated with the Cooper pairing in the superconducting state is of the order of 4.0 meV. This is to be compared with the full gap of 3.6 meV measured in the earlier Angle-Resolved Photoelectron Spectrocopy (ARPES) study (3) and 3.8 meV measured in a recent Scanning Tunneling Microscopy (STM) study (15). In Fig. 5 we compare the temperature dependence of a number of different gaps as a function of temperature. We also show the mean-field temperature dependence of the superconducting gap measured in the close-lying bulk α_2 hole band. The latter is out of range of the present laser study but Δ_0 has been reported elsewhere (16). In plotting $\Delta(T)$ for the bulk band we use the expression

$$\Delta(T) = \Delta_0 \tanh\left[\alpha\left(\frac{T_c}{T} - 1\right)^{1/2}\right], \qquad [5]$$

where α is such that $\Delta_0 = \alpha kT_c$ (17). We are able to make a number of interesting observations from Fig. 5. The temperature dependence of the gap associated with the Dirac point for both the $Te_{0.55}$ and the $Te_{0.7}$ samples follow the bulk superconductivity dependence. The superconducting gap in the topological state at the chemical potential for the $Te_{0.55}$ sample is identical in both the earlier study (3) and the present study and identical to the bulk superconductivity dependence.

Armed with the experimentally determined temperature dependence for the different gaps, we show in Fig. 4 *E–H* representative dispersions calculated from Eq. **3**, to be compared with the experimentally observed behavior shown in Fig. 4 *A–D*. We have not attempted to account for the 3 meV observed above Tc but rather show the opening of the gaps at the Dirac point and at the chemical potential with the onset of superconductivity. The agreement is again quite satisfying. We can make one further important observation regarding the plots shown in Fig. 4 *E–H*. Elsewhere we made reference to the possibility that the gap observed above T_c at the Dirac point could simply be due to sample misalignment (4). However, we note from Fig. 4 *E–H* that as we move to lower binding energy on the Dirac cone, away from the Dirac point, the influence of temperature change occurs at lower and lower temperatures. Further, as we show (*SI Appendix*, section1) there is effectively zero movement of the sample as the temperature is lowered, ruling out any temperature-induced misalignment as the source of any change in gap magnitude.

Our study thus reveals a number of important observations that should stimulate further research and the push for even higher energy resolution. As noted earlier, the opening of a gap at the Dirac point, indicative of time-reversal symmetry breaking, points to the development of some form of ferromagnetic order in the surface region associated with the superconducting transition. Within the Ginsburg–Landau formulism time-reversal symmetry breaking requires mixing between two gap functions resulting in a complex order parameter (*SI Appendix*, section 6). Such a possibility has been discussed before although to date there has been no experimental verification. Through spin–orbit coupling, the complex order parameter can induce spin magnetization as described in *SI Appendix* and explained in detail elsewhere (6). We note that alternative theories that may explain the appearance of the gap at the Dirac point have also been

suggested (18, 19). The presence of ferromagnetism in the surface region associated with strong spin–orbit coupling would potentially make this system an ideal platform for supporting a range of unique topological phenomena.

Materials and Methods

Single crystals of $FeTe_{1-x}Se_x$ were grown by a unidirectional solidification method. The nominal compositions had no excess Fe, and Te, measured by magnetic susceptibility, is 14.5 K in both samples. Single-crystal samples were cleaved in situ at T$\leq$ 5 K and base pressure of $\leq 2 \times 10^{-11}$ Torr. The photoemission studies were carried out using a 3-ps pulse width, 76-MHz repetition rate Coherent Mira 900P Ti:sapphire laser, the output of which was quadrupled to provide 6.0-eV incident light, focused into a spot on the sample ~20 μm in diameter. The polarization of the latter could be varied with the use of quarter and/or half-wave plates to provide linear or circularly polarized light of arbitrary orientation on the Poincaré sphere. Photoemission spectra were obtained using a Scienta SES 2002 electron spectrometer. The effective energy resolution is ~2.5 meV full width at half maximum as determined by the width of the sharpest features in the measured spectra. The angular resolution was ~0.002 $Å^{-1}$ at the low photon energy used. The value of E_F is determined by reference to a gold sample in contact with the $FeTe_xSe_{1-x}$ (FTS) samples.

Data Availability. All study data are included in the article and supporting information.

ACKNOWLEDGMENTS. We acknowledge useful discussions with Igor Zalyznyak, John Tranquada, Dung-Hai Lee, Mike Norman, Lun-Hui Hu, Manfred Sigrist, Weiguo Yin, and Dirk Morr. We also acknowledge excellent technical support from Fran Loeb. The work carried out at Brookhaven was supported in part by the US Department of Energy (DOE) under Contract DE-AC02-98CH10886 and in part by the Center for Computational Design of Functional Strongly Correlated Materials and Theoretical Spectroscopy. C.W. at University of California, San Diego was supported by Air Force Office of Scientific Research (AFOSR) FA9550-14-1-0168. N.Z. was supported by the Comscope project in the initial phase of this project and by the Electron Spectroscopy Field Work Proposal in the later phase.

1. B. Keimer, S. A. Kivelson, M. R. Norman, S. Uchida, J. Zaanen, From quantum matter to high-temperature superconductivity in copper oxides. *Nature* **518**, 179–186 (2015).
2. P. D. Johnson, G. Xu, W.-G. Yin, Eds., *Preface, Iron-Based Superconductivity* (Springer International Publishing, 2015).
3. P. Zhang *et al*., Observation of topological superconductivity on the surface of an iron-based superconductor. *Science* **360**, 182–186 (2018).
4. J. D. Rameau, N. Zaki, G. D. Gu, P. D. Johnson, M. Weinert, Interplay of paramagnetism and topology in the Fe-based high Tc superconductors. *Phys. Rev. B* **99**, 205117 (2019).
5. P. D. Johnson *et al*., Interplay of paramagnetism and topology in the Fe-based high Tc superconductors. *Phys. Rev. Lett.* **114**, 167001 (2015).
6. LH. Hu, P.D. Johnson, C. Wu, Pairing symmetry and topological surface state in iron-chalcgenide superconductors. *Phys. Rev. Res.* **2**, 022021 (2020).
7. X. Wu, S. B. Chung, C. Liu, E.-A. Kim, Topological orders competing for the Dirac surface state in FeSeTe surfaces, *arXiv*:2004.13068 (27 April 2020).
8. U. R. Singh *et al*., Evidence for orbital order and its relation to superconductivity in $FeSe_{0.4}Te_{0.6}$. *Sci. Adv.* **1**, e1500206 (2015).
9. H.-H. Hung *et al*., Anisotropic vortex lattice structures in the FeSe superconductor. *Phys. Rev. B Condens. Matter Mater. Phys.* **85**, 104510 (2012).
10. P. O. Sprau *et al*., Discovery of orbital-selective Cooper pairing in FeSe. *Science* **357**, 75–80 (2017).
11. K. B. Shahar Rinott *et al*., Tuning across the BCS-BEC crossover in the multiband superconductor $Fe_{1+y}Se_xTe_{1-x}$: An angle-resolved photoemission study. *Sci. Adv.* **3**, e1602372 (2017).
12. S. Kasahara *et al*., Giant superconducting fluctuations in the compensated semimetal FeSe at the BCS-BEC crossover. *Nat. Commun.* **7**, 12843 (2016).
13. Y. L. Chen *et al*., Massive Dirac fermion on the surface of a magnetically doped topological insulator. *Science* **329**, 659–662 (2010).
14. E. Mascot, S. Cocklin, S. Rachel, D. Morr, Dimensional tuning of Majorana fermions and real space counting of the Chern number. *Phys. Rev. B* **100**, 184510 (2019).
15. Z. Wang *et al*., Evidence for dispersing 1D Majorana channels in an iron-based superconductor. *Science* **367**, 104–108 (2020).
16. H. Miao *et al*., Isotropic superconducting gaps with enhanced pairing on electron Fermi surfaces in $FeTe_{0.55}Se_{0.45}$. *Phys. Rev. B Condens. Matter Mater. Phys.* **85**, 094506 (2012).
17. T. Dahm, P. J. Hirschfeld, D. J. Scalapino, L. Zhu, Nodal quasiparticle lifetimes in cuprate superconductors. *Phys. Rev. B Condens. Matter Mater. Phys.* **72**, 214512 (2005).
18. A. Ghazaryan, P. L. S. Lopes, P. Hosur, M. J. Gilbert, P. Ghaemi, Effect of Zeeman coupling on the Majorana vortex modes in iron-based topological superconductors. *Phys. Rev. B* **101**, 020504 (2020).
19. J. L. Lado, M. Sigrist, Detecting nonunitary multiorbital superconductivity with Dirac points at finite energies. *Phys. Rev. Res.* **1**, 033107 (2019).